Genetically Encoded Molecular Biosensors To Image Histone Methylation in Living Animals

Thillai V. Sekar,[†] Kira Foygel,[†] Juri G. Gelovani,[‡] and Ramasamy Paulmurugan*,[†]

[†]Molecular Imaging Program at Stanford, Bio-X Program, Stanford University School of Medicine, 318 Campus Drive, East Wing, 1st Floor, Stanford, California 94305, United States

[‡]Department of Biomedical Engineering, College of Engineering, and Center for Molecular Medicine and Genetics, School of Medicine, Wayne State University, 1400 Chrysler Freeway, Detroit, Michigan 48207, United States

S *Supporting Information*

ABSTRACT: Post-translational addition of methyl groups to the amino terminal tails of histone proteins regulates cellular gene expression at various stages of development and the pathogenesis of cellular diseases, including cancer. Several enzymes that modulate these post-translational modifications of histones are promising targets for development of small molecule drugs. However, there is no promising real-time histone methylation detection tool currently available to screen and validate potential small molecule histone methylation modulators in small animal models. With this in mind, we developed genetically encoded molecular biosensors based on the split-enzyme complementation approach for in vitro and in vivo imaging of lysine 9 (H3−K9 sensor) and lysine 27 (H3−K27 sensor) methylation marks of histone 3. These methylation sensors were validated in vitro in HEK293T, HepG2, and HeLa cells. The efficiency of the histone methylation sensor was assessed by employing methyltransferase inhibitors (Bix01294 and UNC0638), demethylase inhibitor (JIB-04), and siRNA silencing at the endogenous histone K9-methyltransferase enzyme level. Furthermore, noninvasive bioluminescence imaging of histone methylation sensors confirmed the potential of these sensors in monitoring histone methylation status in response to histone methyltransferase inhibitors in living animals. Experimental results confirmed that the developed H3−K9 and H3−K27 sensors are specific and sensitive to image the drug-induced histone methylation changes in living animals. These novel histone methylation sensors can facilitate the in vitro screening and in vivo characterization of new histone methyltransferase inhibitors and accelerate the pace of introduction of epigenetic therapies into the clinic.
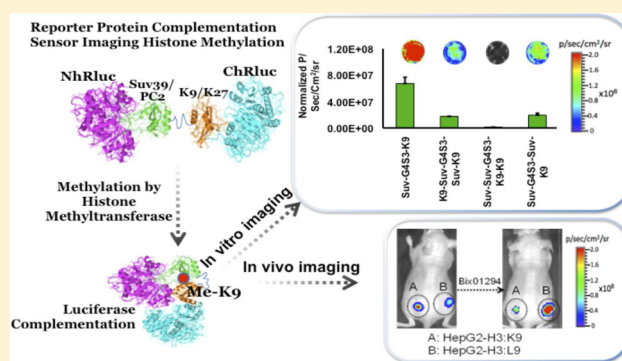
E pigenetics is a rapidly expanding area of biomedical research that studies phenomena of heritable changes in genome functions that occur without changes in the underlying DNA sequence. The epigenetic mechanisms, such as DNA-methylation, histone acetylation, and histone methylation, are important for cellular development, differentiation, proliferation, and apoptosis.[1,2] Furthermore, the epigenetic mechanisms are believed to respond to different chemical and physical agents, and may lead to altered biological pathways associated with cellular diseases.[3] More recent discoveries on functional mechanisms of epigenetic processes indicate that most of these epigenetic processes are heritable.[4,5] Although most of the epigenetic processes are heritable, recent findings have confirmed that they are also *reversible*, making them potentially valuable therapeutic targets in treating various diseases.

One of the important epigenetic mechanisms involves methylation of histone core proteins H3 and H4 by methyltransferases, particularly on the side-chain nitrogen atoms of lysine and/or arginine residues.[6] Lysine methylation predominantly occurs in K4, K9, K27, K36, and K79 of histone

3 (H3), and K20 of histone 4 (H4). Histone methylations such as H3−K9, H3−K27, and H4−K20 are mainly involved in the formation and maintenance of silent heterochromatin state, whereas methylations at H3−K4, H3−K36, and H3−K79 are associated with actively transcribing euchromatic regions.[7] Although acetylation directly correlates with transcriptional activation, histone lysine methylation can be involved in both transcriptional activation and repression.[8]

The heterochromatic complex is essential for chromosome organization, maintenance of genomic integrity, and inheritance. H3−K9 methylation was shown to be predominantly associated with heterochromatin formation, particularly with X-chromosome inactivation and DNA methylation.[9] To a certain extent, the H3−K9 methylation is also associated with transcriptional regulation of some important genes.[10] The functional effects of histone lysine methylations are mediated

by various effector proteins, which possess methylated lysine-binding chromodomains. The specificity of chromodomains of effector proteins in binding to methylated lysine residues of histone proteins is so accurate that they can even distinguish the location of methylated lysines and the number of methylations (mono-, di-, or tri-) occurring in each of these lysine residues.[11] The methylation of lysine residues by histone methyltransferases (HMTs) recruits chromodomain of different proteins, which recognize and form a complex that can functionally remodel chromatin structure and regulate gene expression in response to the external stimuli.[12,13] Most interestingly, histone modifications are *reversible*; the balance between N-tail histone methylation and demethylation in lysine and arginine residues at different positions can regulate expression levels of different proteins and control cellular homeostasis.[14] It is now clearly understood that by regulating histone methylation, the gene expression profile of a cell can be manipulated. Several conventional methods are currently available to detect methylation levels of histone proteins in cell lysates, but none of them could be employed for real-time monitoring of histone methylation status of cells in living animals.[15,16] Addition of a new efficient imaging strategy could accelerate the process of development and preclinical evaluation of novel inhibitors of histone methyltransferases.

In the current study, we used split-Renilla luciferase complementation system to develop sensors, which can image methylation in H3−K9 and H3−K27 marks. We constructed plasmid vectors expressing these sensor fusion proteins to monitor methylations occurring at specific locations in N-terminal tail of histone proteins (K9 and K27). These sensors become activated when either the K9 or K27 become methylated and bind with the Suv39H1 or Pc2 domains that bring two halves of split-RLuc together, reconstitute its enzymatic activity, and activate bioluminescence that can be imaged in cells in vitro, and in vivo in living animals. The functionality and specificity of these histone methylation sensors was successfully demonstrated in response to methyltransferase and demethylase inhibitors in cell lines, and noninvasive repetitive bioluminescence imaging in living animals.

■ MATERIALS AND METHODS

Plasmid Vector Construction. Fusion constructs were generated by cloning PCR-amplified cDNA of Suv39H1 and Pc2 with pcDNA3.1 (+) eukaryotic expression vector into Kpn1 and BamH1 restriction sites, followed by the incorporation of K9- and K27-sensor oligonucleotides into EcoR1 and Xho1 sites and the $(G_4S)_3$ linker sequence (GGGGSGGGGSGGGGS) at BamH1 and EcoR1 sites in between Suv39H1 and K9 sensor peptide sequence. The entire fusion was flanked by N- and C-terminal fragments of Renilla luciferase 8.6 (RLuc8.6) and Renilla luciferase (RLuc) respectively. H3−K9 and H3−K27 mutant clones were generated by replacing codon for lysine with leucine. Full length FLuc express under a constitutive ubiquitin promoter was used for cotransfection.

Refer to the Supporting Information for additional methods

■ RESULTS AND DISCUSSION

Design, Construction, and Optimization of Bioluminescent Histone Methylation Imaging Sensors in Cells. We adopted the concept of intramolecular conforma-

tional change that occurs within a protein in response to post-translational modifications, such as phosphorylation, methylation, acetylation, and so forth, to design our split-reporter complementation-based histone methylation sensors (Figure 1). The versatility of the split reporter complementation system
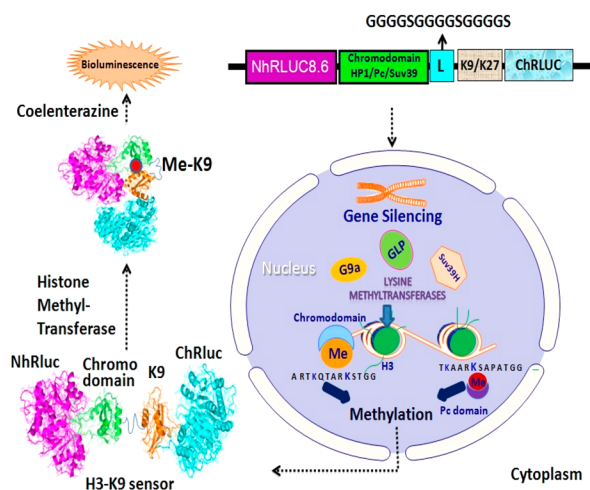

Figure 1. Schematic illustration of the concept and the design of histone methylation imaging sensor.

has been shown by our previous studies in imaging protein−protein interactions and protein folding.[17−21] Recently split-reporters has been extended to study various epigenetic modifications such as phosphorylation,[22,23] ubiquitylation,[24] and DNA methylation[25] that occurs in cells. In addition to the use of split-reporter complementation systems, Kanno et al. developed a FRET sensor to detect histone acetylation,[26] whereas Lin et al. used the FRET sensor to image histone methylation[15] in live cells. Similarly, a few other fluorescent-based probes have been developed to image histone acetylation in cells and small animals.[27,28] In this study, we extended the potential of split reporter complementation system to image protein methylation by Renilla luciferase (RLuc) complementation system. The H3−K9 and H3−K27 methylation sensors were constructed independently using substrate domains (K9: ARTKQTAR**K**STGG; K27: TKAAR**K**SAPATGG) derived from histone 3 (H3). Chromodomain derived from either HP1 protein or histone-lysine *N*-methyltransferase (Suv39H1) was used for the K9 sensor, and polycomb protein 2 (Pc2) was used for the K27 sensor, as interacting partners (Supporting Information Figure S1). A flexible linker with three time repeats of GGGGS ($[G_4S]_3$) was used to link the methylation domain and the interacting substrate domain, in order to facilitate the proximity interaction of these domains during complementation. The sensors were sandwiched between N- and C-terminal domains of the split-Renilla luciferase protein (RLuc8.6) so that optimal enzyme complementation could be achieved as the result of interaction of methylated K9 or K27 peptides with corresponding methyl-lysine binding domains of HP1, Pc2, or Suv39H1. The system was studied in transfected mammalian cells. The dissociation constant of methylated H3−K9 peptide with HP1 chromodomain has been reported to be 2.14 μM as assessed by Nuclear Magnetic Resonance.[29] Similarly, the binding constant assessed by isothermal calorimetric titration assay for HP1 has been estimated to be 7 μM for dimethyl H3−K9 peptide and 2.5 μM for trimethyl H3−K9 peptide.[30] The H3−K9 sensor developed in the present study is expressed
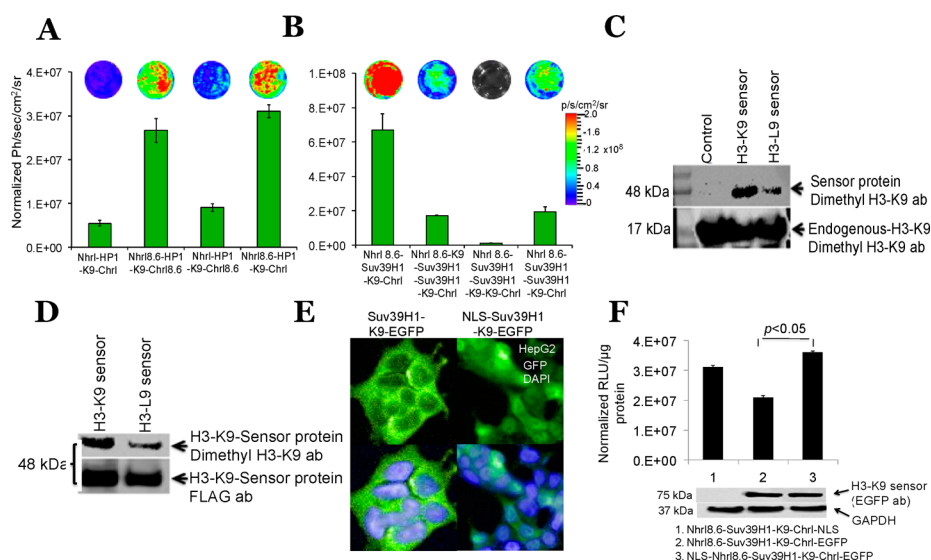
Figure 2. Optimization of split-RLuc fragments. (A) RLuc signal measured from HEK293T-cells transfected with complementation sensors constructed with HP1 and K9-interacting partners with N- and C-terminal RLuc fragments from humanized (NhRL and ChRL) or red-shifted mutant RLuc (NhRL8.6 and ChRL8.6). (B) Optimal number of H3−K9-peptide and the chromodomain needed to achieve efficient sensor signal: RLuc signal measured from HEK293T-cells transfected with complementation sensors constructed with K9 peptide from H3 protein and interacting chromodomain from Suv39H1, in various copy numbers tested for sensors efficiency in measuring histone methylation. (C) Immunoblot analysis of H3−K9-sensor methylation detected by methylation specific antibody: The upper panel shows the wild-type and mutant sensor proteins detected from the immunoprecipitated samples by H3−K9 dimethyl antibody, and the lower panel shows the endogenous H3−K9 proteins detected from the cell lysates of respective samples by the same antibody. (D) H3−K9-sensor methylation detected by methylation specific antibodies after immunoprecipitation: The upper panel shows the wild-type and mutant sensor proteins detected with H3−K9 dimethyl antibody, and the lower panel shows the sensor proteins detected by FLAG antibody. (E) Fluorescence images show the localization of NLS-bearing methylation sensor tagged with EGFP-fusion in the nucleus. (F) Upper panel shows RLuc signal measured from HEK293T cells transfected with complementation sensor-EGFP-fusions with and without NLS shown in (E). Lower panel shows the immunoblot analysis of cell lysates of respective samples in graph using EGFP antibody. GAPDH expression was used to normalize the results. In all experiments, the constructs with RLuc reporter fragments and the interacting protein fragments are in the order they appear in the X-axis labels.

approximately at 15 μM in transfected cells (calculated using the band intensity of Western blot analysis of sensor proteins by FLAG antibody by comparing with tubulin[31]). Further, the sensor generates signal by interacting through intramolecular interaction of methylated H3−K9 peptide and chromodomain positioned within the same fusion protein. Therefore, the H3−K9 sensor developed in this study is capable of generating significant luciferase signal upon methylation and also can respond to changes in the level of methylation. However, this evaluation may have some variations because binding affinity of antibodies used for various target proteins in Western blot analysis is different.

In general, histone 3 with K9 methylation is abundant in transcriptionally repressive heterochromatic regions.[32] This process occurs through interaction of K9-methylated histone 3 with the chromodomain of heterochromatin-associated protein 1 (HP1). Considering the sensitivity, initially we constructed H3−K9 (ARTKQTARKSTGG) and its respective mutant (H3-L9: ARTKQTARLSTGG) sensors using substrate chromodomain from HP1 protein, and the split-Renilla luciferase fragments of selective split site at amino acid position 229 (NhRLuc: 1−229; ChRLuc: 229−311). The sequence-confirmed vectors were studied in transiently transfected HEK293T cells by assaying for reconstituted RLuc activity. The results revealed an approximately 20-fold difference between the H3−K9 and H3−L9 sensor (5 ± 0.5 x10^6 photons/sec vs 2.5 ± 0.5 x10^5 photons/sec). The background photon flux was 1.2 ± 0.2 x10^5 photons/sec. Because the aim of this study was to develop a sensor that could image histone methylation status in living animals, we further improved the

sensitivity of the sensor by testing the N- and C-terminal fragments of a red-shifted (emission: 535 nm) mutant RLuc (RLuc8.6$_{535}$), which we have previously developed for improved RLuc protein stability.[33] We generated four different sensor constructs with rational N- and C-terminal luciferase fragment combinations (Supporting Information Figure S1), and we tested them in transfected HEK293T cells. The results showed a 4-fold increase in sensor signal when NhRLuc fragment in the initial sensor was replaced with NhRLuc8.6 [(Figure 2A), Nhrl-HP1-K9-Chrl vs Nhrl8.6-HP1-K9-Chrl)]. We used this particular combination of N- and C-terminal luciferase fragments for additional optimizations and for constructing various other sensors (H3−K9 and H3−K27) that were employed in this study. The maximum luminescence spectrum (λ-max) of Nhrl8.6-HP1-K9-Chrl matched with the emission spectrum of RLuc8.6$_{535}$ (Supporting Information Figure S2).

After our initial evaluation of H3−K9 sensor with chromodomain from HP1, a complex responsible for heterochromatin formation, we assessed the functional specificity of these sensors by introducing chromodomains from other proteins, which are involved in transcriptional regulation of gene expression. We selected chromodomain from polycomb 2 (Pc2) and suppressor of variegation 3-9 homologue 1 (Suv39H1). The Pc2 protein is mainly associated with transcriptionally repressive chromatin, especially in X-chromosome inactivation, by interacting with methylated histone 3 at K27.[34] The polycomb group (PcG) of proteins has recently been identified to interact with Suv39H1 through methylated H3−K9, and is involved in transcriptional

repression in other active complexes. Suv39H1 is a histone-lysine *N*-methyltransferase enzyme that possesses the chromo-domain and the SET domain, which can interact with H3 protein while methylating K9. The vectors expressing H3−K9 sensor with chromodomain from HP1 and Suv39H1, and H3−K27 sensor with Pc2-chromodomain was studied in transiently transfected HEK293T cells and assessed for reconstituted RLuc bioluminescence activity. The results demonstrated significant levels of bioluminescent signal from H3−K9 sensor consisting of chromodomain from Suv39H1 and H3−K27 sensor consisting of Pc2 chromodomain (Supporting Information Figure S3). The sensor containing the HP1 chromodomain showed a low level of bioluminescent signal. Although the levels of bioluminescent signals from reconstituted RLuc were different for different sensors, the expression levels of individual sensor proteins did not differ significantly in the transfected cells.

Because the chromodomains of Suv39H1 and HP1 are known to interact with both di- and tri-methylated H3−K9,[35−37] the complementation signal measured in this study is a combination of signals achieved from the interaction of chromodomains with both di- and tri-methylated H3−K9. The mono, di-, and tri-methylation in the H3−K9 mark by different histone methyl transferases controls chromatin organization in cells at various cellular conditions. Although trimethylation in the H3−K9 mark recruits HP1 and contributes for condensed heterochromatin, the mono- and di-methylations of the same have been associated with regulatory repressive function in euchromatic regions.[38,39]

Furthermore, when trimethylation of H3−K9 by Suv39H1 methyltransferase recruits the HP1 chromodomain to regulate heterochromatin, mono- and di- methylation of the same mark by G9a methyltransferase regulates selective repression of gene expression in euchromatic regions during embryonic develop-ment.[40] Hence the broad specificity of the split reporter complementation sensor with the chromodomains from Suv39H1 and HP1 is useful in measuring global methylation status of the H3−K9 mark, but it is not capable to distinguish the specific degree of methylations in this particular mark. Further investigations by replacing Suv39H1 chromodomain with other domains from the royal family of proteins[40] can improve the specificity of the H3−K9 sensor capable of detecting mono-, di-, and tri-methylation of the H3−K9 mark discretely to screen small molecule drugs altering a specific degree of H3−K9 methylation implicated in various cellular diseases.[41]

To further test the hypothesis that increasing the number of chromodomains and K9 substrate peptide domains could improve sensor imaging signal, we generated three additional constructs in which we either duplicated both K9 and Suv39H1 domains [K9-Suv39H1-$(G_4S)_3$-Suv39H1-K9 and Suv39H1-Suv39H1-$(G_4S)_3$-K9-K9], or duplicated only the chromodo-main alone [Suv39H1-$(G_4S)_3$-Suv39H1-K9] (Supporting In-formation Figure S1); these sensor constructs were studied in transiently transfected HEK293T cells. The multiplication of interacting domains in these sensors resulted significant drop in bioluminescence signals from all the tested multidomain sensor constructs (Figure 2B). Therefore, for the rest of the studies, we used constructs containing only one pair of interacting partners.

To validate whether it is possible to detect methylation of the K9 domain positioned within the imaging sensor by methylation-specific H3−K9-antibody, we constructed wild type and mutant sensors with C-terminal FLAG peptide sequence to facilitate selective immunoprecipitation and further confirmation. No significant differences in the absolute level of protein expression were observed other than a minor drop in bioluminescence signals when comparing sensors with and without C-terminal FLAG peptide fusion (Supporting Information Figure S4A,B).

The proteins from cell lysates of HEK293T cells transfected with equal amounts of vector constructs expressing H3−K9 or respective mutant (H3−L9) sensors immunoprecipitated by FLAG specific antibody, were detectable with anti-Dimethyl-K9 and anti-FLAG specific antibodies. The endogenous dimethyl-ated K9 of H3-protein from the whole cell lysates of the respective samples was also detectable by anti-Dimethyl-K9 antibody (Figure 2C,D and Figure S4B). We also observed some level of sensor protein in H3−L9 transfected cells, which might be due to the nonspecific nature of Dimethyl-K9 antibody used for immunoblot analysis.

Effect of Nuclear Localization Signal (NLS) Peptide on H3−K9 Methylation Sensor Signal. Histone methylations are enzymatic processes that occur in the nucleus and are executed by histone methyltransferases.[6,7] Histone methyl-transferases are predominantly located in the nucleus. HP1, Pc2, and Suv39H1 are chromodomain-containing proteins that possess inherent nuclear localization signal peptide within their protein sequence. Although, the protein fragments with chromodomains derived from these nuclear proteins could mediate nuclear translocation of sensor proteins and help sensors achieve histone methylations, we tested whether the addition of NLS signal peptide to these sensor proteins can improve sensor signal. Therefore, we constructed additional vectors that express sensor proteins with NLS signal peptide tagged in the C-terminus (NhRluc8.6-Suv39H1−H3−K9-ChRLuc-NLS and NhRluc8.6-Suv39H1−H3-L9-ChRLuc-NLS) and sensors with C-terminal EGFP- with and without N-terminal NLS tag (NhRLuc8.6-Suv39H1−H3−K9-ChRLuc-EGFP and NLS-NhRLuc8.6-Suv39H1−H3−K9-ChRLuc-EGFP) (Supporting Information Figure S1). HEK293T cells were transfected to stably express these sensors and the subcellular localization of EGFP-tagged sensor proteins was analyzed using confocal microscopy. Confocal microscopy clearly showed the distribution of EGFP signal mostly in the cytoplasm of cells expressing sensor without NLS, whereas cells expressing the sensor with NLS showed signal both in the nucleus and cytoplasm (Figure 2E). Importantly, the addition of NLS resulted in a significant improvement in sensitivity of histone methylation sensors as manifested by a 30 ± 5% increase in reconstituted luciferase activity (Figure 2F, upper panel). Therefore, we used plasmid constructs expressing H3−K9 and H3−L9 sensor proteins with NLS at C-terminal end of the protein further for all in vitro and in vivo experiments. Immunoblot analysis by EGFP specific antibody showed no variation in the levels of sensor proteins from cells expressing the sensor with or without NLS signal peptide (Figure 2F, lower panel).

Specificity of Split-Luciferase Complementation Sen-sor in Measuring Histone Methylations. After diligent optimization of different components of the methylation sensor proteins to improve their sensitivity, we then evaluated the specificity of histone methylations as measured by these optimized sensors. Initially we constructed respective mutant sensors (H3−L9 and H3−L27) by changing amino acid lysine within the methylation domain of the sensor proteins to leucine

(K → L). Similarly, we constructed a mutant H3−K9 sensor in which amino acid tryptophan within the chromodomain Suv39H1 that is crucial for interaction with the methylated H3−K9 was mutated to alanine (W64A, W74A). The constructs were transfected in HEK293T cells and assessed for reconstituted luciferase activity. Our results demonstrated significantly lower level of complemented luciferase signal from the sensors when amino acid lysine in respective positions (K9 and K27) of the sensors was mutated to leucine (L9 and L27; ($p < 0.01$)). The H3−K9 sensor signal ($5.26 \pm 1.2 \times 10^6$ RLU/μg protein) was 8 ± 2 fold higher than its respective mutant H3−L9 sensor ($5.96 \pm 1.5 \times 10^5$ RLU/μg protein) (Figure 3A). Similarly, the H3−K27 sensor with its interacting

Suv39H2, GLP, SETDB1, and SETDB2) can also methylate H3−K9.[42] To study the effect of G9a methyltransferase (EHMT2) on H3−K9 sensor methylation, we selected siRNA-mediated gene silencing. We tested H3−K9 methylation sensor using luciferase assay (Figure 3D), bioluminescence imaging (Figure 3E), immunoblot analysis for endogenous G9a methyltransferase and methylated H3−K9 sensor protein level (Figure 3F) after transfecting the HEK293T cells with 6 μM of siRNA specific to G9a methyltransferase or scrambled siRNA. As a result, a significant correlation was observed between G9a methyltransferase level and sensor signal (Figure 3G).

Evaluation of H3−K9 and H3−K27 Methylation Sensors in Different Cell Lines. Methylation status of histones (H3 and H4) varies with the amount of specific methyltransferases and demethylases expressed in cells. To determine the efficiency and the generalizability of H3−K9 and H3−K27 methylation sensors, we evaluated them in different cell lines such as HEK293T-human embryonic kidney cancer cells, HepG2 hepatocellular carcinoma cells, and HeLa ovarian cancer cells. Plasmid constructs expressing H3−K9 and H3−K27 with respective mutant sensors (H3−L9 and H3−L27) were transiently transfected, and the level of bioluminescence signals was not uniform across various cell lines included in the study (Supporting Information Figure S5).

H3−K9 Methylation Sensors in Response to the Treatment of Different Doses of Methyltransferase and Demethylase Inhibitors. To evaluate the efficiency of the methylation sensors in response to methyltransferase inhibitors, we created HEK293T cells stably expressing the sensors, and we treated them with two different methyltransferase inhibitors (Bix01294 and UNC0638). The optimal concentration of these methyltransferase inhibitors was determined by subjecting cells to various concentrations (Bix01294:0, 1, 2, 3, 4, and 5 μM; UNC0638:0, 0.25, 0.5, 1, 2, and 4 μM) followed by measuring luciferase complementation after 24 and 48 h of incubation. The Hill equation with variable slope in GraphPad Prism 6 ((GraphPad Software, CA): $Y = \text{Bottom} + (\text{Top} - \text{Bottom})/(1 + 10\wedge((\text{LogIC50} - X) * \text{HillSlope}))$) was used for Figure 4A and C, and exponential decay regression was used to fit the results for Figure 4B and D. The results of these studies demonstrated inhibitor concentration-dependent decrease in luciferase reconstitution in cells expressing H3−K9 sensor (Bix01294: $R^2 = 0.9$ and UNC0638: $R^2 = 0.87$). In contrast, cells expressing mutant sensor (H3−L9) showed no relationship between the magnitudes of bioluminescence signal and the concentration of inhibitors used for the study (Figure 4A−D). Additionally, HEK293T cells expressing H3−K9 sensor showed a concentration-dependent increase in luciferase signal when treated with increasing concentrations of JIB-04, a demethylase inhibitor (Figure 4E). Lastly, the methylation imaging signal was proportional to various concentrations of methyltransferase and demethylase inhibitors used in this study.

Imaging Histone Methylation in Living Animals. The complementation sensors we developed for this study were sensitive and robust in measuring histone methylations in cell cultures. We further tested the feasibility of noninvasive imaging of histone methylation status in vivo in nude mice bearing tumor xenografts developed from different tumor cells expressing H3−K9 sensor. Because in vivo imaging requires another independent normalization of bioluminescence signal intensity, we used all cell lines expressing the H3−K9 and H3−L9 (mutant) sensors cotransfected with firefly luciferase
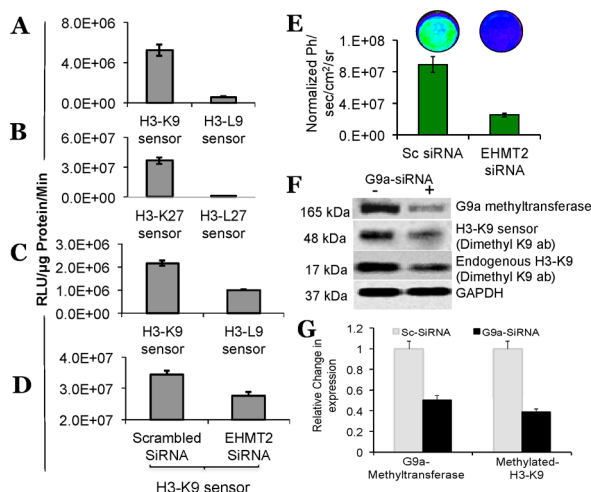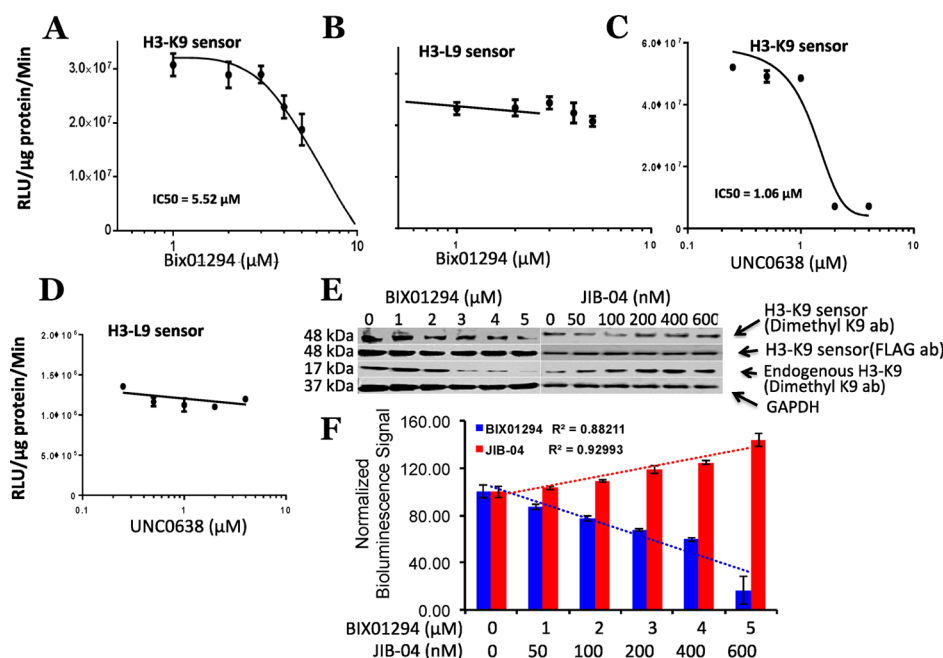

Figure 3. Specificity of histone methylation sensors. (A) RLuc signal measured from HEK293T cells transfected with H3−K9 wild-type and mutant complementation sensors. (B) RLuc signal measured from HEK293T cells transfected with H3−K27 and H3−L27 sensors with no NLS. (C) RLuc signal measured from HEK293T cells transfected with H3−K9 wild-type and Suv39H1 mutant (tryptophan at amino acid locations 64 and 74 was replaced with alanine) sensors. (D) RLuc signal measured from stable HEK293T cells expressing H3−K9 sensor transfected with scrambled and G9a specific SiRNAs. (E) RLuc signal measured in stable HEK293T cells expressing H3−K9 sensor transfected with scrambled and G9a specific siRNAs. (F) Immunoblot shows the level of dimethylated-H3−K9 sensor, endogenous dimethylated H3−K9, and G9a-methyltransferase measured in HEK293T cells transfected with SiRNA specific to G9a and scrambled-SiRNA. (G) Figure shows the change in the level of G9a-methyltransferase and dimethylated H3−K9 in HEK293T cells transfected with SiRNA specific to G9a-methyltransferase and scrambled-SiRNA.

chromodomain from Pc2 protein was 80 ± 10 times higher ($3.67 \pm 0.5 \times 10^7$ RLU/μg protein) than its respective mutant H3−L27 sensor ($3.15 \pm 0.5 \times 10^5$ RLU/μg protein) (Figure 3B). Moreover, the H3−K9 sensor with the mutated Suv39H1 chromodomain ($1.75 \pm 0.17 \times 10^6$) showed more than 50% drop in luciferase complementation as compared to the H3−K9 sensor with wild-type Suv39H1 chromodomain ($3.3 \pm 0.38 \times 10^6$) (Figure 3C).

To further confirm the specificity of sensor complementation in relation to the endogenous expression level for histone methyltransferases, we used the H3−K9 sensor. The G9a histone methyltransferase is mainly involved in methylating histone protein 3 at the K9-position.[39] In addition to G9a methyltransferase, several other methyltransferases (Suv39H1,

Figure 4. Evaluation of histone methylation sensors (H3−K9 and H3−L9) in response to the treatment of different doses of methyltransferase and demethylase inhibitors in HEK293T cells stably expressing the sensors. (A) RLuc signal measured from stable HEK293T cells expressing H3−K9 sensor exposed to various concentrations (0 to 5.0 μM) of Bix01294. (B) RLuc signal measured from stable HEK293T cells expressing H3−L9 sensor exposed to various concentrations (0 to 5.0 μM) of Bix01294. (C) RLuc signal measured from stable HEK293T cells expressing H3−K9 sensor exposed to various concentrations (0 to 4.0 μM) of UNC0638. (D) RLuc signal measured from stable HEK293T cells expressing H3−L9 sensor exposed to various concentrations (0 to 4.0 μM) of UNC0638. (E) Immunoblot analysis of lysates of HEK293T cells stably expressing H3−K9 sensor treated with different doses of methyltransferase inhibitor (Bix01294) and demethylase inhibitor (JIB-04), for expressed H3−K9 sensor level, dimethylated fraction of H3−K9 sensor level, and endogenous dimethylated H3−K9 level. GAPDH was used to normalize the results. Dimethylated H3−K9 sensor protein was detected after immunoprecipitation of cell lysates using the tagged FLAG specific antibody. (F) RLuc sensor signal measured from HEK293T cells stably expressing H3−K9 sensor after treated with different doses of methyltransferase inhibitor (Bix01294) and demethylase inhibitor (JIB-04). Concentrations of Bix01294 and JIB-04 are labeled on the *X*-axis.

reporter under a constitutive ubiquitin promoter. The double-selected cells of respective sensors with clones of cells that expressed an equal amount of FLuc at both the mRNA and protein levels and showed an equal growth rate were used for animal experiments (Supporting Information Figure S6). The HEK293T, HeLa, and HepG2 cells stably coexpressing each methylation sensor (H3−K9 or H3−L9) along with FLuc (10^6 cells per xenograft) were implanted subcutaneously in the right (H3−K9) and left (H3−L9) flanks of nude mice, and the mice were housed according to standard maintenance protocol until tumors grew to 2−3 mm in diameter. Thereafter, repetitive bioluminescence imaging was performed to assess histone methylation status in tumor-bearing mice until tumors reached 10 mm in diameter. The results of this study demonstrated the feasibility of monitoring histone methylation status by non-invasive bioluminescence imaging. The in vivo bioluminescence imaging from animals implanted with HEK293 (Figure 5A,B) and HeLa (Figure 5C,D) cells showed 8 ± 2-fold higher luciferase signal from cells expressing H3−K9 sensor when compared to cells expressing its respective mutant sensor (H3−L9). The utilization of the dual-luciferase imaging approach enabled us to reliably quantify the magnitude of down-regulation of histone methylation in tumor tissue induced by treatment of mice with histone methyltransferase inhibitors in vivo.

We further tested H3−K9 complementation sensor in response to G9a methyltransferase inhibitor Bix01294 in animals implanted with xenograft of HepG2 cells stably expressing H3−K9 and H3−L9 sensors along with equal
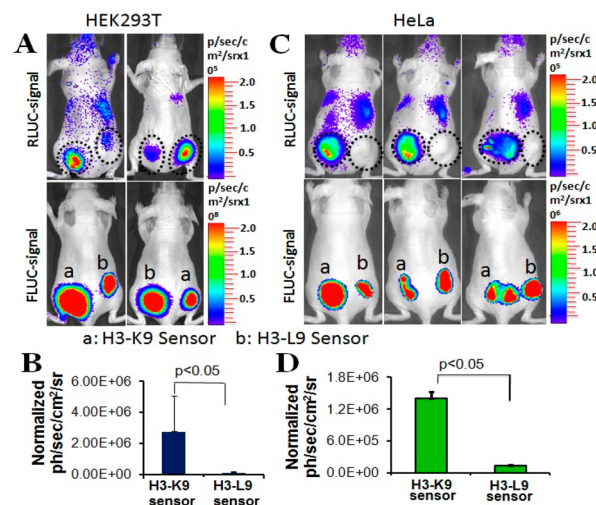

Figure 5. In vivo imaging of histone methylation in the nude mice model. (A) RLuc and FLuc signals of HEK293T xenograft expressing H3−K9 and H3−L9 sensors. (B) Normalized histone methylation assisted Renilla luciferase complementation signal measured from HEK293T xenograft expressing wild-type and mutant sensors. (C) RLuc and FLuc signals optically imaged from the tumor xenografts of HeLa cells stably expressing wild-type and mutant histone methylation sensors. (D) Normalized histone methylation assisted RLuc signal measured from HeLa xenograft expressing wild-type and mutant sensors.

level of FLuc reporter for normalization. Intratumoral injection of either PBS or Bix01294 (5 µL of 1 mg/mL Bix01294 in three different sites of tumor) in HepG2 tumors of 2−3 mm diameter were imaged as before, and 24 h after the injection of Bix01294 injection for both RLuc (methylation sensor signal) and FLuc (normalization) signals. The result shows a significant level of drop in luciferase complementation ($40 \pm 8\%$) in tumors from animals expressing H3−K9 sensor upon receiving Bix01294 ($p < 0.05$). In contrast, the tumors from animals receiving PBS showed ∼80% increase in luciferase signal (Supporting Information Figure S7).

CONCLUSION

Global methylations of specific histone marks are shown to be altered in different types of cancers,[41] and therefore, tuning a specific methylation mark seems a promising therapeutic strategy. A plethora of small molecules are explored to modulate specific histone methylation marks, and also, research endeavors are underway to introduce highly efficacious small molecule histone methylation modulators. The pace of small molecule exploration is stalled due to the shortage of tools to detect and monitor the methylation status of specific histone methylation marks and preclinically validates them for quick clinical translation. In this study, we developed and optimized novel methylation sensors for noninvasive bioluminescence imaging of particular histone methylation process in cell extracts, intact cells, and noninvasively in living animals by using cells genetically engineered to express these sensors. Furthermore, we confirmed the efficacy of these sensors using noninvasive bioluminescence imaging for monitoring of pharmacodynamics of different histone methyltransferase inhibitors in vivo in mice bearing tumor xenografts of cells engineered to express these novel histone methylation sensors. Preclinical utilization of these histone methylation sensors can facilitate the in vitro screening and in vivo characterization of novel histone methyltransferase inhibitors and accelerate the pace of introducing epigenetic therapies into the clinic.

ASSOCIATED CONTENT

Ⓢ Supporting Information

Supplementary methods and figures. This material is available free of charge via the Internet at http://pubs.acs.org.

AUTHOR INFORMATION

Corresponding Author

*Email: paulmur8@stanford.edu. Phone: 650-725-6097. Fax: 650-721-6921.

Author Contributions

T.V.S. and R.P designed and performed the experiments and wrote the manuscript. K.F. assisted to perform experiments and helped manuscript writing. J.G.G assisted design and manuscript correction.

Notes

The authors declare no competing financial interest.

ACKNOWLEDGMENTS

REFERENCES

(1) Cohen, I.; Poreba, E.; Kamieniarz, K.; Schneider, R. *Genes Cancer* **2011**, *2*, 631−647.

(2) Sharma, S.; Kelly, T. K.; Jones, P. A. *Carcinogenesis* **2010**, *31*, 27−36.

(3) Herceg, Z.; Vaissiere, T. *Epigenetics* **2011**, *6*, 804−819.

(4) Margueron, R.; Reinberg, D. *Nat. Rev. Genet* **2010**, *11*, 285−296.

(5) Bell, J. T.; Spector, T. D. *Trends Genet.* **2011**, *27*, 116−125.

(6) Kouzarides, T. *Cell* **2007**, *128*, 693−705.

(7) Kouzarides, T. *Cell* **2007**, *128*, 802.

(8) Sims, R. J., III; Nishioka, K.; Reinberg, D. *Trends Genet.* **2003**, *19*, 629−639.

(9) Bartova, E.; Krejci, J.; Harnicarova, A.; Galiova, G.; Kozubek, S. *J. Histochem. Cytochem.* **2008**, *56*, 711−721.

(10) Richards, E. J.; Elgin, S. C. *Cell* **2002**, *108*, 489−500.

(11) Izzo, A.; Schneider, R. *Briefings Funct. Genomics* **2010**, *9*, 429−443.

(12) Jones, D. O.; Cowell, I. G.; Singh, P. B. *Bioessays* **2000**, *22*, 124−137.

(13) Platero, J. S.; Hartnett, T.; Eissenberg, J. C. *EMBO J.* **1995**, *14*, 3977−3986.

(14) Varier, R. A.; Timmers, H. T. *Biochim. Biophys. Acta* **2011**, *1815*, 75−89.

(15) Lin, C. W.; Jao, C. Y.; Ting, A. Y. *J. Am. Chem. Soc.* **2004**, *126*, 5982−5983.

(16) Weiss, T.; Hergeth, S.; Zeissler, U.; Izzo, A.; Tropberger, P.; Zee, B. M.; Dundr, M.; Garcia, B. A.; Daujat, S.; Schneider, R. *Epigenetics Chromatin* **2010**, *3*, 7.

(17) Paulmurugan, R.; Gambhir, S. S. *Proc. Natl. Acad. Sci. U.S.A.* **2006**, *103*, 15883−15888.

(18) Massoud, T. F.; Paulmurugan, R.; Gambhir, S. S. *Nat. Med.* **2010**, *16*, 921−926.

(19) Paulmurugan, R.; Gambhir, S. S. *Anal. Chem.* **2007**, *79*, 2346−2353.

(20) Paulmurugan, R.; Gambhir, S. S. *Anal. Chem.* **2005**, *77*, 1295−1302.

(21) Paulmurugan, R.; Gambhir, S. S. *Anal. Chem.* **2003**, *75*, 1584−1589.

(22) Herbst, K. J.; Allen, M. D.; Zhang, J. *J. Am. Chem. Soc.* **2011**, *133*, 5676−5679.

(23) Spotts, J. M.; Dolmetsch, R. E.; Greenberg, M. E. *Proc. Natl. Acad. Sci. U.S.A.* **2002**, *99*, 15142−15147.

(24) Chen, Z.; Zhong, Y.; Wang, Y.; Xu, S.; Liu, Z.; Baskakov, I. V.; Monteiro, M. J.; Karbowski, M.; Shen, Y.; Fang, S. *PLoS One* **2013**, *8*, e73482.

(25) Badran, A. H.; Furman, J. L.; Ma, A. S.; Comi, T. J.; Porter, J. R.; Ghosh, I. *Anal. Chem.* **2011**, *83*, 7151−7157.

(26) Kanno, T.; Kanno, Y.; Siegel, R. M.; Jang, M. K.; Lenardo, M. J.; Ozato, K. *Molecular Cell* **2004**, *13*, 33−43.

(27) Sato, Y.; Mukai, M.; Ueda, J.; Muraki, M.; Stasevich, T. J.; Horikoshi, N.; Kujirai, T.; Kita, H.; Kimura, T.; Hira, S.; Okada, Y.; Hayashi-Takanaka, Y.; Obuse, C.; Kurumizaka, H.; Kawahara, A.; Yamagata, K.; Nozaki, N.; Kimura, H. *Sci. Rep.* **2013**, *3*, 2436.

(28) Sasaki, K.; Ito, A.; Yoshida, M. *Bioorg. Med. Chem.* **2012**, *20*, 1887−1892.

(29) Nielsen, P. R.; Nietlispach, D.; Mott, H. R.; Callaghan, J.; Bannister, A.; Kouzarides, T.; Murzin, A. G.; Murzina, N. V.; Laue, E. D. *Nature* **2002**, *416*, 103−107.

(30) Jacobs, S. A.; Khorasanizadeh, S. *Science* **2002**, *295*, 2080−2083.

(31) Gard, D. L.; Kirschner, M. W. *J. Cell Biol.* **1987**, *105*, 2191−2201.

(32) Stewart, M. D.; Li, J.; Wong, J. *Mol. Cell. Biol.* **2005**, *25*, 2525−2538.

(33) Loening, A. M.; Wu, A. M.; Gambhir, S. S. *Nat. Methods* **2007**, *4*, 641−643.

(34) Simon, J. A.; Kingston, R. E. *Molecular Cell* **2013**, *49*, 808−824.

(35) Wang, T.; Xu, C.; Liu, Y.; Fan, K.; Li, Z.; Sun, X.; Ouyang, H.; Zhang, X.; Zhang, J.; Li, Y.; Mackenzie, F.; Min, J.; Tu, X. *PLoS One* **2012**, *7*, e52977.

(36) Kim, J.; Daniel, J.; Espejo, A.; Lake, A.; Krishna, M.; Xia, L.; Zhang, Y.; Bedford, M. T. *EMBO Rep.* **2006**, *7*, 397−403.

(37) Bannister, A. J.; Zegerman, P.; Partridge, J. F.; Miska, E. A.; Thomas, J. O.; Allshire, R. C.; Kouzarides, T. *Nature* **2001**, *410*, 120−124.

(38) Shinkai, Y.; Tachibana, M. *Genes Dev.* **2011**, *25*, 781−788.

(39) Tachibana, M.; Ueda, J.; Fukuda, M.; Takeda, N.; Ohta, T.; Iwanari, H.; Sakihama, T.; Kodama, T.; Hamakubo, T.; Shinkai, Y. *Genes Dev.* **2005**, *19*, 815−826.

(40) Yap, K. L.; Zhou, M. M. *Biochemistry* **2011**, *50*, 1966−1980.

(41) Greer, E. L.; Shi, Y. *Nat. Rev. Genet.* **2012**, *13*, 343−357.

(42) Wu, H.; Min, J.; Lunin, V. V.; Antoshenko, T.; Dombrovski, L.; Zeng, H.; Allali-Hassani, A.; Campagna-Slater, V.; Vedadi, M.; Arrowsmith, C. H.; Plotnikov, A. N.; Schapira, M. *PLoS One* **2010**, *5*, e8570.